

# Preparation and in vitro apatite-forming ability of porous and non-porous titania microspheres

Zhixia LI,<sup>†</sup> Toshiki MIYAZAKI\* and Masakazu KAWASHITA\*\*

School of Chemistry and Chemical Engineering, Guangxi University, 100 Daxue Road, Xixiangtang, Nanning 530004, China

\*Graduate School of Life Science and Systems Engineering, Kyushu Institute of Technology,  
2-4 Hibikino, Wakamatsu-ku, Kitakyushu 808-0196, Japan

\*\*Graduate School of Biomedical Engineering, Tohoku University, 6-6-11-901-4 Aramaki-Aoba, Aoba, Sendai 980-8579, Japan

Porous and non-porous titania microspheres with the anatase or rutile phase were successively prepared by the sol-gel process followed by heat treatment at various temperatures. The pore size of the prepared microspheres was effectively controlled by incorporating silica nanoparticles of different diameters. The apatite-forming ability of the microspheres was investigated in a simulated body fluid, with ion concentrations nearly equal to those of human blood plasma. Results indicated that the titania microspheres with either anatase or rutile structure induced the formation of calcium phosphate compounds (CaPs) on the microsphere surface. The deposition of CaPs was more pronounced on the TiO<sub>2</sub> microspheres calcined at 600°C (anatase structure) and 800°C (rutile structure), compared to that calcined at 500°C (anatase structure). Additionally, anatase microspheres with smooth surface and low specific surface area favored the formation of CaPs, compared to porous microspheres. This indicates that nanoscale pores do not essentially favor apatite formation.

©2013 The Ceramic Society of Japan. All rights reserved.

Key-words : Titania microspheres, Apatite, Anatase, Rutile, Calcium phosphate compounds

[Received May 15, 2013; Accepted July 1, 2013]

## 1. Introduction

Tissue engineering and regenerative medicine aim to restore damaged tissues using a combination of functional cells and biodegradable scaffolds made from engineered biomaterials. Some of the most promising biomaterials actively used in bone tissue engineering include bioactive glasses, glass-ceramics, titanium and its alloys, due to their ability to form tenacious bonds with the bone. The bone integration, also known as osseointegration property, of these biomaterials originates through the formation of bone-like hydroxyapatite layers upon reacting with physiological fluids, leading to effective biological interaction and fixation of bone tissue with the material surface.<sup>1-3)</sup> In particular, sol-gel-derived titania (TiO<sub>2</sub>) coatings and silica (SiO<sub>2</sub>) coating have been reported to exhibit bioactivity when dispersed in simulated body fluid (SBF).<sup>2),3)</sup> Following that, several studies were devoted to unravel the mechanism underlying the nucleation of apatite on TiO<sub>2</sub> and SiO<sub>2</sub> coatings. These studies indicated that certain hydroxyl groups such as Si-OH and Ti-OH are responsible for the generation of hydroxyapatite, by providing sites for calcium phosphate nucleation.<sup>4-7)</sup> Among them, Ti-OH in the titania gel with an anatase structure has been reported to be remarkably effective in inducing apatite nucleation in SBF.<sup>8)-10)</sup>

Recently, studies were performed to compare the apatite formation on TiO<sub>2</sub> film with smooth surface (with anatase structure) and porous surface. The results demonstrated that porous TiO<sub>2</sub> film with granular surface and anatase structure showed enhanced capability for apatite formation.<sup>11)</sup> This implies that the chemistry and topography of the implant surface greatly influences its bone-bonding ability. In addition, several studies were conducted

to analyze the relationship between porosity and bioactivity of the implants. For example, titanium with macroporous surface was reported to exhibit improved bone-bonding strength.<sup>12),13)</sup> Furthermore, sol-gel-derived SiO<sub>2</sub> and CaO-P<sub>2</sub>O<sub>5</sub>-SiO<sub>2</sub> coatings with mesoporous (2 nm < pore size < 50 nm) surface was reported to have enhanced the nucleation of hydroxycarbonate apatite.<sup>2)</sup> These findings illustrate the requirement of suitable porous structure for improving the bioactivity of implants.

For injectable biomaterials, a spherical shape is more advantageous, as their geometry allows them to be delivered more easily through needles. In particular, porous microspheres possess unique characteristics, such as low density, high hydrophilic property, making them ideally suitable for use as drug carriers in the developing drug delivery systems (DDS).<sup>14)</sup> To the best of our knowledge, only very few works have focused on dispersed TiO<sub>2</sub> microspheres with controlled pore size and volume. Hence in this study, porous and non-porous TiO<sub>2</sub> microspheres were prepared by the sol-gel process, and their apatite-forming ability was investigated in SBF. The crystallinity of TiO<sub>2</sub> microspheres was controlled by heat treatment at various temperatures. We believe that the results derived from this study will open up new opportunities for designing biomaterials for tissue engineering applications.

## 2. Experimental procedure

### 2.1 Materials

Analytical-grade titanium tetraisopropoxide (TTIP), diethanolamine (DEA), methanol (CH<sub>3</sub>OH), kerosene, sorbitan monooleate (span 80), and sorbitan monostearate (span 60) supplied by Wako Pure Chemical Industries, Japan, were used as reagents. Colloidal silica particles with an average particle diameter of 15 nm (Snowtex 40), 50 nm (Snowtex XL), and 200 nm (indigenously-made), were used as template to control the pore size of

<sup>†</sup> Corresponding author: Z. Li; E-mail: zhixiali@hotmail.com

TiO<sub>2</sub> microspheres. Snowtex 40 and Snowtex XL were supplied by Nissan Chemical Industries, LTD., Japan.

Silica particles of diameter 200 nm were prepared as follows: 2.5 g of tetraethoxysilane (Wako Pure Chemical Industries) and 7 mL of ammonia solution (concentration: 28%) were dispersed separately in 35 mL of 2-methoxyethanol (Wako Pure Chemical Industries) to form solution A and solution B, respectively. Following that, solution B was added slowly into solution A, under constant stirring at 5000 rpm. The resulting mixture was aged for 30 min at room temperature. Finally, silica particles with an average diameter of 200 nm were separated out by centrifuging the aged suspension at 6000 rpm.

## 2.2 Preparation of microspheres

TiO<sub>2</sub> microspheres were prepared by a sol-gel process, starting from TTIP in water-in-oil emulsion. The water phase was composed of TTIP, DEA, CH<sub>3</sub>OH, and water, at a molar ratio of TTIP/DEA/CH<sub>3</sub>OH/H<sub>2</sub>O = 1:1.7:7.5:20.8. Oil phase was composed of kerosene containing 18 wt% of surfactant. The surfactant consisted of span 80 and span 60 in the weight ratio of span 80/span60 = 3:1. Gelation was initiated by stirring the resulting mixture at 1800 rpm and stepwise emulsification at 40°C for 20 min, 50°C for 20 min, and 60°C for 140 min. After completion of the reaction, the as-obtained gel microspheres were separated by centrifugation at 3000 rpm. The microspheres were then washed with ethanol, and dried at 60°C for 12 h. The dried gel particles were then calcined at 500, 600, and 800°C for 5 h, for controlling the desired crystalline phase, followed by dispersing them in 3 M NaOH solution at room temperature for 24 h. Finally, the obtained microspheres were washed with ultra-pure water, and dried at 60°C for 12 h.

Porous TiO<sub>2</sub> microspheres were prepared using the method similar to that described above, with some modifications described as follows. In the initial water phase, 10% colloidal silica particles were substituted for water. Prior to mixing with the solution of TTIP, DEA, and CH<sub>3</sub>OH, the pH of the colloidal silica particles was adjusted to 7 with 1 M hydrochloric acid. Subsequently, incorporation of colloidal silica nanoparticles of diameter 15, 50, and 200 nm resulted in samples P-15, P-50, and P-200, respectively.

## 2.3 Dispersion of the microspheres in SBF

The SBF with ion concentrations (Na<sup>+</sup> 142.0, K<sup>+</sup> 5.0, Ca<sup>2+</sup> 2.5, Mg<sup>2+</sup> 1.5, Cl<sup>-</sup> 147.8, HCO<sub>3</sub><sup>-</sup> 4.2, HPO<sub>4</sub><sup>2-</sup> 1.0, SO<sub>4</sub><sup>2-</sup> 0.5 mM), nearly equal to those in human blood plasma,<sup>15),16)</sup> was prepared by dissolving reagent-grade CaCl<sub>2</sub>, K<sub>2</sub>HPO<sub>4</sub>·3H<sub>2</sub>O, KCl, NaCl, MgCl<sub>2</sub>·6H<sub>2</sub>O, NaHCO<sub>3</sub> and Na<sub>2</sub>SO<sub>4</sub> (Nacalai Tesque) in ultra-pure water, and buffered at pH 7.4 using tris(hydroxymethyl)aminomethane [(CH<sub>2</sub>OH)<sub>3</sub>CNH<sub>2</sub>, Nacalai Tesque] and 1 M HCl (Nacalai Tesque) at 36.5°C. In a polystyrene bottle, 0.03 g of the TiO<sub>2</sub> microspheres was dispersed in 14 mL of the prepared acellular SBF. The bottle containing microspheres dispersed SBF was fixed on a rotator and rotated at 3 rpm/min at 36.5°C. The SBF in bottle was refreshed every two days. After a given time period, the microspheres were separated from the SBF, gently washed with ultra-pure water, and dried at 60°C.

## 2.4 Characterization of microspheres

The crystalline phase of the samples was verified by powder X-ray diffraction (XRD; RINT-2200VL, Rigaku, Japan). The morphology and particle size were observed by using scanning electron microscope (SEM; VE-8800, Keyence, Japan), transmission electron microscopy (TEM; HF2000, Hitachi, Japan) and

energy dispersive X-ray analysis (EDX; Noran, USA). Chemical composition of sample was analyzed by Fourier transform infrared spectrometer (FT-IR; FT/IR-6200, Jasco, Japan), by recording transmission spectra using potassium bromide (KBr) pellet method. The content of the testing sample in KBr pellets was kept at around 0.5 wt%. The specific surface area of the samples was determined by the BET method using nitrogen adsorption-desorption isotherm at 77 K on a Micromeritics ASAP 2020 instrument (USA). Zeta potentials of the samples were characterized by using laser electrophoresis spectroscopy (Model ELS-Z, Otsuka Electronics Co., Japan) at various pH values in 142 mM NaCl solution, which has same Na<sup>+</sup> and Cl<sup>-</sup> concentrations as that in SBF. The pH of the NaCl solution was adjusted using 1 M HCl or NaOH aqueous solution.

## 3. Results

Figure 1 shows the SEM images of the microspheres obtained by calcination at 600°C, before and after dispersion in NaOH solution. It could be observed that, irrespective of the nature of silica particles in the colloidal solution, the resulting TiO<sub>2</sub> particles were spherical in shape. With regard to the particle size, the TiO<sub>2</sub>, P-50, and P-200 samples had a mean diameter of about 5 μm, while P-15 had a smaller diameter (about 2–3 μm). As can be observed in the SEM images, the prepared TiO<sub>2</sub> particles had a smooth surface, which became rough with the incorporation of silica particles during the preparation process. Furthermore, it was observed that the dispersion of the samples P-200, P-50, and P-15 in NaOH resulted in a porous surface. It was realized that the pore sizes was similar to the diameter of the incorporated silica nanoparticles. The specific surface area of the prepared

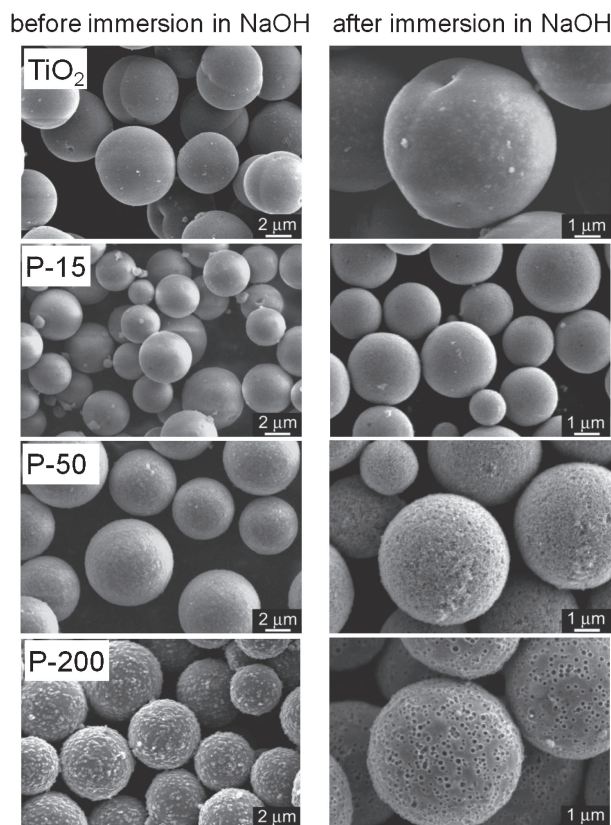


Fig. 1. SEM photographs of TiO<sub>2</sub> microspheres and porous TiO<sub>2</sub> microspheres heated at 600°C before and after dispersion in 3M NaOH solution.

samples is listed in **Table 1**. It could be observed that the specific surface area of porous microspheres greatly increased with decrease in the diameter of incorporated silica nanoparticles.

**Figures 2(a)–2(c)** and **2(g)** show the FT-IR spectra of P-200, P-50, P-15, and TiO<sub>2</sub>, respectively, before dispersion in NaOH. Similarly, **Figs. 2(d)–2(f)** and **2(h)** show the FT-IR spectra of P-200, P-50, P-15, and TiO<sub>2</sub>, respectively, after dispersion in NaOH. The FTIR spectra of the samples P-200, P-50, and P-15, before dispersion in NaOH, showed an absorption band at 1100 cm<sup>-1</sup>. This could be attributed to the Si–O–Si asymmetrical stretching.<sup>17)</sup> However, this band disappeared in the FTIR spectra of the samples P-200, P-50, and P-15, after dispersion in NaOH. This indicates that the removal or dissolution of silica nanoparticles upon dispersion in NaOH. Additionally, for all porous TiO<sub>2</sub> microspheres, the FTIR spectra exhibited an absorption

Table 1. Specific surface area of porous and non porous TiO<sub>2</sub> microspheres heated at 600°C

Sample	Specific Surface Area (m <sup>2</sup> /g)
TiO <sub>2</sub>	6.4
P-15	145.0
P-50	72.5
P-200	57.1

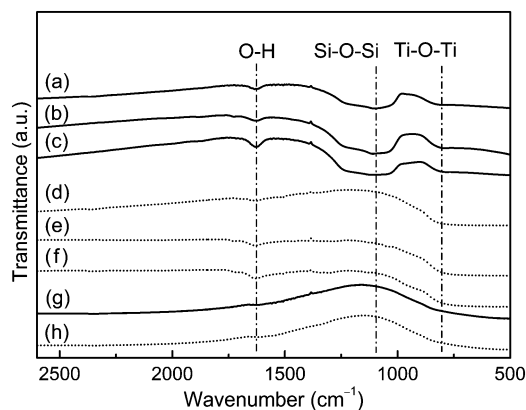


Fig. 2. FT-IR spectra of porous and nonporous TiO<sub>2</sub> microspheres heated at 600°C before and after dispersion in 3M NaOH. (a) P-200, (b) P-50, (c) P-15 and (g) TiO<sub>2</sub> are before dispersion in NaOH; (d) P-200, (e) P-50, (f) P-15 and (h) TiO<sub>2</sub> are after dispersion in NaOH.

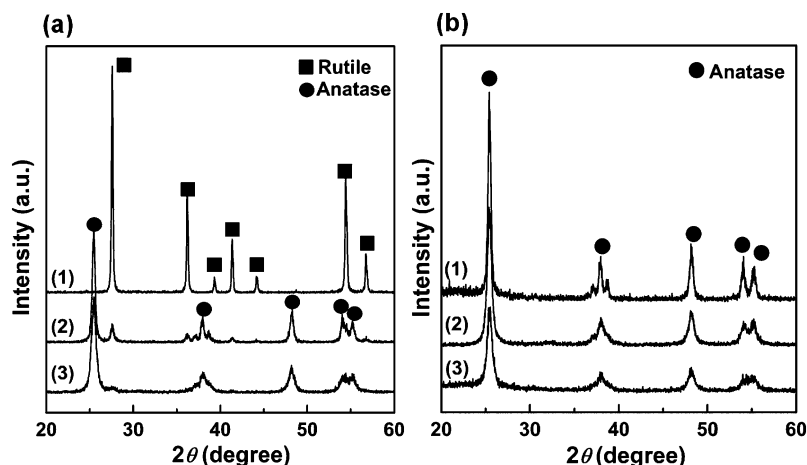


Fig. 3. XRD patterns of (a) TiO<sub>2</sub> and (b) P-50 microspheres heated at temperatures of (1) 800°C, (2) 600°C, and (3) 500°C.

peak at 1630 cm<sup>-1</sup>, corresponding to O–H bending vibration of water molecules.<sup>18)</sup> Nevertheless, no obvious difference could be observed in the FT-IR spectra of TiO<sub>2</sub> microspheres before and after dispersion in NaOH. These results suggest that the hydrophilicity of microspheres, which is one of the desired properties of injectable biomaterials, increased due to the incorporation of silica nanoparticles.

**Figure 3** shows the XRD patterns of the samples TiO<sub>2</sub> and P-50 calcined at 500, 600, and 800°C for 3h. As can be observed in Fig. 3(a), the microspheres were mainly composed of anatase phase, when the calcination temperature was below 600°C. On calcination at 800°C, the rutile phase became dominant.<sup>19),20)</sup> On the other hand, the XRD patterns in Fig. 3(b) indicated that the sample P-50 exhibited pure anatase phase, even after heating at different temperatures. The sample P-15 also showed XRD patterns similar to that of P-50 (data not shown), exhibiting pure anatase phase. In case of sample P-200, the XRD pattern exhibited both anatase and rutile phases upon heating at 800°C, and pure anatase phase for heat treatments below 600°C (not shown here). These results indicate that the incorporation of silica nanoparticles in titania microspheres inhibited the formation of the rutile phase during the heat treatment.<sup>21)</sup>

**Figure 4** shows the SEM images of the TiO<sub>2</sub> microsphere surface, obtained by heating at 500, 600, and 800°C, and after dispersion in SBF for 4 days and 8 days. It could be observed that island-like spherulites were deposited on the surface of all the TiO<sub>2</sub> samples dispersed in SBF for 4 days. The spherulites were found to gradually overspread throughout the surfaces, after dispersion in SBF for 8 days. The newly formed spherulite layer, on the TiO<sub>2</sub> microspheres heated at 600 and 800°C, were observed to be more pronounced and uniform.

**Figure 5** shows the surface morphology of the porous TiO<sub>2</sub> microspheres heated at 600°C, after dispersion in SBF for 8 days. This was compared with that of TiO<sub>2</sub> microspheres heated at 500°C. Compared to non-porous TiO<sub>2</sub> microspheres [Fig. 5(a)], only small amount of spherulites were observed on the surface of the porous microspheres (P-15, P-50, P-200) after dispersion in SBF [Figs. 5 (b)–5(d)]. In addition, in case of porous microspheres, it was observed that the spherulites were deposited in the gap between the microspheres.

**Figure 6(a)** shows the XRD patterns of TiO<sub>2</sub> microspheres heated at various temperatures after dispersion in SBF for 8 days. **Figure 6(b)** shows XRD patterns of porous TiO<sub>2</sub> microspheres (P-15, P-50 and P-200) with an anatase structure, after dispersion in SBF for 8 days. The XRD pattern of TiO<sub>2</sub> microspheres is also

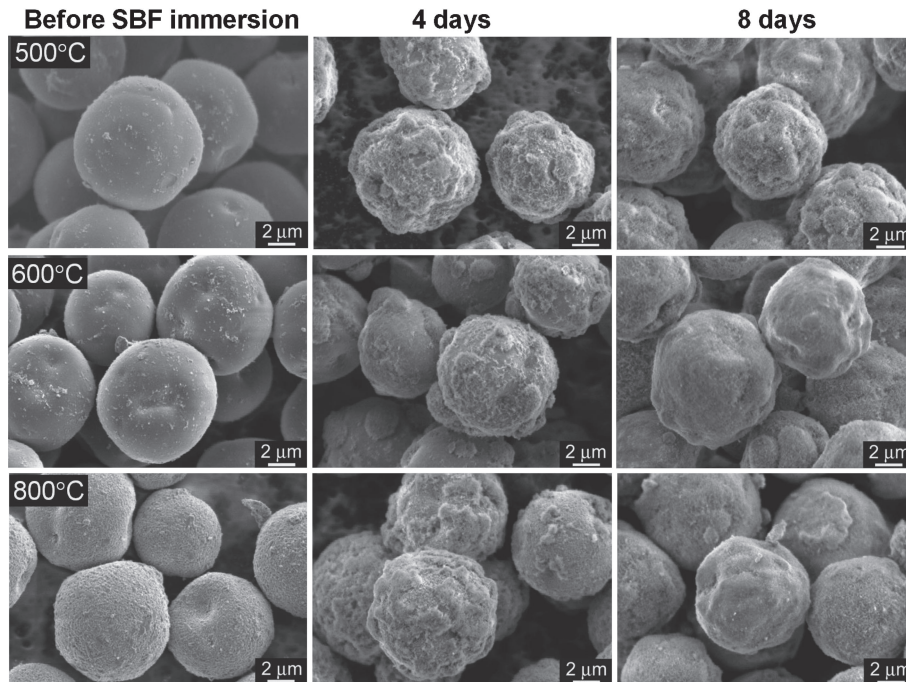


Fig. 4. SEM photographs of surface of  $\text{TiO}_2$  microspheres heated at various temperatures before and after dispersion in SBF for 4 days and 8 days.

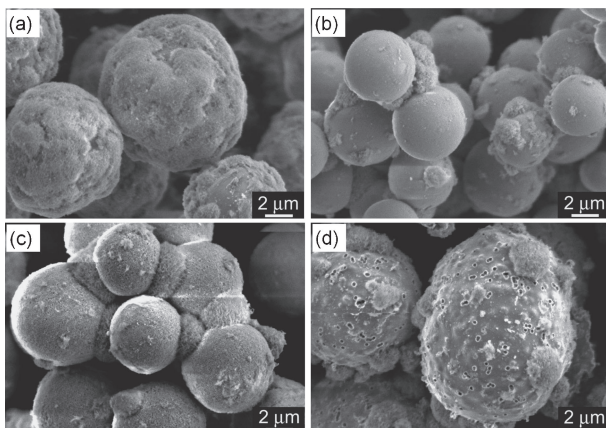


Fig. 5. SEM photographs of surfaces of porous  $\text{TiO}_2$  microspheres heated at  $600^\circ\text{C}$  after dispersion in SBF for 8 days, which were compared with  $\text{TiO}_2$  microspheres heated at  $500^\circ\text{C}$ , (a)  $\text{TiO}_2$ ; (b) P-15; (c) P-50; (d) P-200.

shown in Fig. 6(b) for comparison. The XRD patterns of all the samples exhibited broad peak around  $2\theta$  values of  $32^\circ$ , indicating that the newly formed layer consisted of superfine crystalline and/or defective grains.<sup>22)</sup> Furthermore, an additional diffraction peak around  $26^\circ$  was observed in the case of microspheres heated at  $800^\circ\text{C}$  [Fig. 6(a)], while it was not clearly observed in the case of microspheres heated at 600 and  $500^\circ\text{C}$ , which had an anatase structure. This could be attributed to the masking effect of the strong diffraction peak of anatase near  $26^\circ$ . These diffraction patterns were so weak in intensity that it was difficult to identify any crystalline phase from these patterns clearly.

Figure 7 shows the (a) TEM images, (b) electron diffraction patterns, and (c) EDX profiles of the surfaces of  $\text{TiO}_2$  and P-200, after dispersion in SBF for 8 days. The TEM images indicated that a more uniform layer was deposited on the surface of  $\text{TiO}_2$ ,

while island-like spherulites were deposited on the surface of P-200. In addition, polycrystalline diffraction rings were observed on the surface of both  $\text{TiO}_2$  and P-200, as shown in Fig. 7(b). The most two visible rings could be regarded as octacalcium phosphate (OCP) rings of (002) and (402) or hydroxyapatite (HA) rings of (002) and (211), even though it is considered controversial to perform phase identification from TEM ring patterns.<sup>23)</sup> Quantitative EDX analysis of the newly formed spherulite layer on  $\text{TiO}_2$  and P-200 surfaces showed that the relative amount of Ca/P was 1.25 and 1.54, respectively. Nevertheless, the Ca/P atomic ratio in both the samples ( $\text{TiO}_2$  and P-200) were much lower than that of bone apatite (Ca/P = 1.65) and stoichiometric hydroxyapatite [ $\text{Ca}_{10}(\text{PO}_4)_6(\text{OH})_2$ ] (Ca/P = 1.67).<sup>24),25)</sup> The newly formed spherulite layers, since their calcium phosphate compositions cannot be confirmed by present data, will be referred to as “CaPs” in the forthcoming sections.

#### 4. Discussion

It is apparent from the above results that the titania microsphere with the anatase or rutile phase can induce CaPs formation on its surface. Moreover, the deposition of CaPs was more uniform on the rutile microspheres derived by heat treatment at  $800^\circ\text{C}$ , than on anatase microspheres obtained by heat treatment at  $500^\circ\text{C}$  (see Figs. 3 and 4). Nancollas et al. have explained the nucleation of calcium phosphates on anatase and rutile surfaces based on the surface tension. According to his report, anatase has higher apatite-forming ability compared to rutile.<sup>26)</sup> In the present study, the surface of rutile microspheres favored the formation of more uniform CaPs layer, which could be attributed to its rugged surface structure, formed as a result of heat treatment at  $800^\circ\text{C}$  (Fig. 4).

Figure 8 shows the zeta potentials for the samples  $\text{TiO}_2$  and P-50 as a function of pH in 142 mM NaCl solution. It was found that the surface of both  $\text{TiO}_2$  and P-50 exhibited negative zeta potentials. In fact, the surface of P-50 was more negatively charged, after dispersion in SBF. Based on this negative zeta

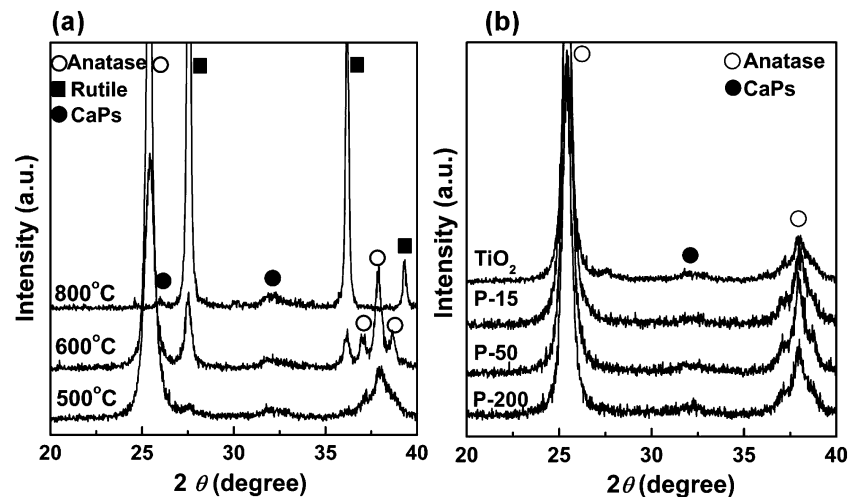


Fig. 6. XRD patterns of (a)  $\text{TiO}_2$  microspheres heated at various temperatures, and (b) porous  $\text{TiO}_2$  microspheres with an anatase structure, after dispersion in SBF for 8 days.

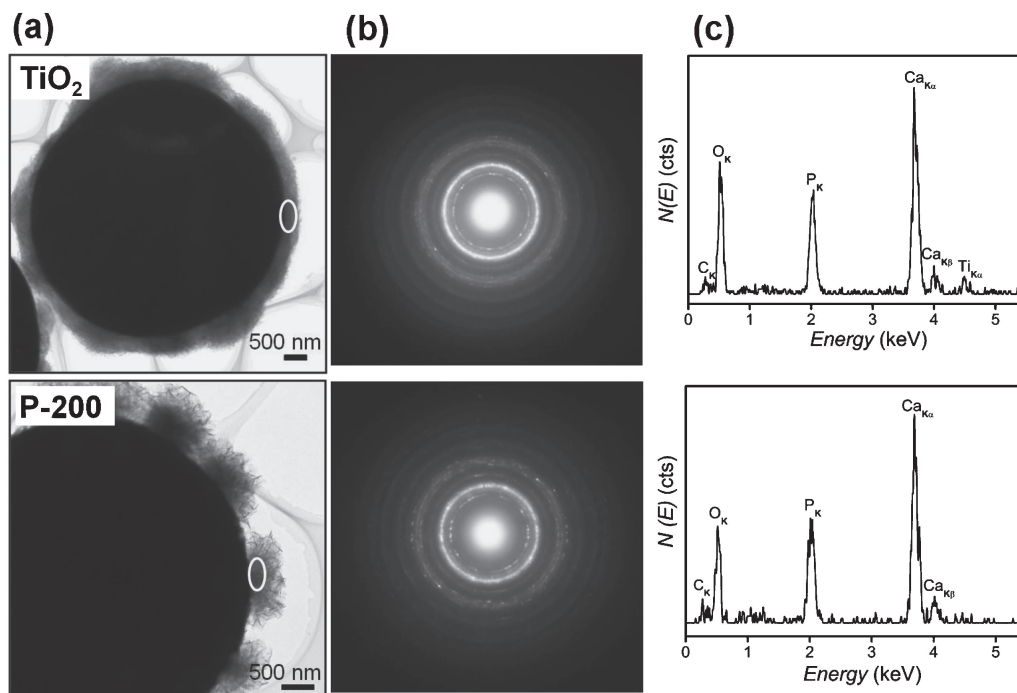


Fig. 7. (a) TEM images, (b) electron diffraction patterns, and (c) EDX profiles of the surfaces of  $\text{TiO}_2$  and P-200, after dispersion in SBF for 8 days.

potential, the mechanism underlying the nucleation of CaPs on the microsphere surface, could be explained as follows: the negative  $\text{TiO}_2$  surface attracts positively charged calcium ions and these calcium ions later combine with phosphate ions in the fluid to form CaPs with a low Ca/P ratio.<sup>8),27),28)</sup> At the same time, the sample P-50, which had a more negatively charged surface, induced lesser CaPs. This implies that, in addition to zeta potential, certain other factors could affect the formation of CaPs.

As listed in Table 1, porous microspheres had a higher surface area compared to non-porous  $\text{TiO}_2$  microspheres. However, CaPs tend to deposit favorably on non-porous  $\text{TiO}_2$  microspheres, when dispersion in SBF. This might probably be due to the amount of ions in SBF, which might be insufficient for efficient nucleation of apatite throughout the high surface area porous microspheres. Therefore, SBF was refreshed every two days and

1.5 SBF was also used to replace SBF. As a result, a similar trend was observed in the case of dispersion in 1.5 SBF. These results indicate that, for a micron-sized particle, surface area might not influence the nucleation of apatite on its surface.

Previous study has reported that high mesopore volume and wide mesopore size distribution accelerates the formation of hydroxycarbonate apatite on porous sol-gel-derived  $\text{SiO}_2$  and  $\text{CaO-P}_2\text{O}_5\text{-SiO}_2$  substrates.<sup>2)</sup> However, in present study, P-15 and P-50 showed predominantly mesoporous structure, but did not favor the formation of CaPs on their surface, even upon dispersion in SBF up to 8 days. This indicates that the presence of mesopores did not play a role in inducing apatite nucleation in the present system. According to Zener et al., a low solute concentration region is present in the solution near the solid surface, during the solid-liquid reaction. The thickness of this region is

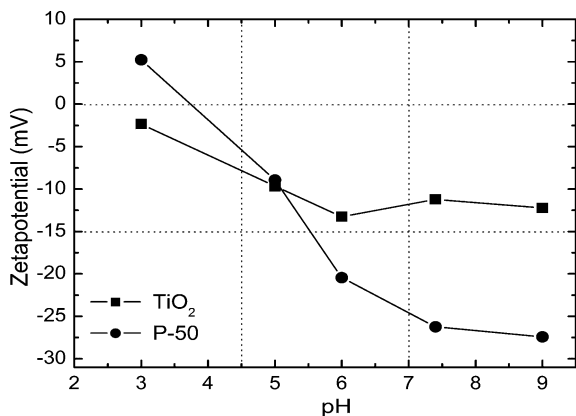


Fig. 8. Zeta potentials for TiO<sub>2</sub> and porous TiO<sub>2</sub> (P-50) particles as a function of pH in 142 mM NaCl solution.

controlled by the reaction rate and the diffusion coefficient of the solute in the solution.<sup>29)</sup> Moreover, Liang et al. have studied the relationship between apatite formation and the pore size in porous titanium. According to them, if the pore size is bigger, the solute could reach the bottom of the pores easily. This favors the growth of apatite nuclei, since they can absorb Ca<sup>2+</sup> and HPO<sub>4</sub><sup>2-</sup> continuously. On the other hand, if the pore size is smaller, the bottom is shielded by the low solute concentration region, which is not beneficial for the nucleation and growth of apatite.<sup>30)</sup> Therefore, in the present study, the nanosized pores on the surface of the samples did not favor the nucleation of apatite. In addition to these factors, the pore shape, e.g. closed pore (not connected between pores) or open pore (interconnected), could possibly affect the apatite nucleation significantly. Further investigations are still needed to clarify the effect of pore size and pore shape on the apatite formation on microsphere surface.

## 5. Conclusions

Porous and non-porous titania microspheres were prepared successfully, and the in-vitro apatite-forming ability of the prepared microspheres was evaluated by dispersing them in SBF. It was found that, upon dispersion in SBF, either the anatase or rutile phase can induce the formation of calcium phosphate compounds (CaPs) on the surface of the microspheres. Non-porous anatase microspheres induced the formation of more uniform CaPs layers, compared to porous microspheres with nanoscale porosity. Further, highly negative zeta potential and high surface area did not promote the CaPs formation on microsphere surface. Rather, pore size and pore shape could be important factors influencing the formation of apatite.

**Acknowledgements** This study was partially supported by National Natural Science Foundation of China (Project 21266002); the Scientific Research Foundation of GuangXi University (Grant No. XGZ120081); Grant-in-Aid for JSPS Fellows from the Japan Society for the Promotion of Science (JSPS). The authors thank to Dr. Maeda, Graduate School of Environmental Science, Tohoku University, for surface area measurement of samples.

## References

- 1) L. L. Hench, *J. Am. Ceram. Soc.*, **74**, 1487–1510 (1991).
- 2) T. Peltola, M. Jokinen, H. Rahiala, E. Levänen, J. B.

- Rosenholm, I. Kangasniemi and A. Yli-Urpo, *J. Biomed. Mater. Res.*, **44**, 12–21 (1999).
- 3) T. Peltola, M. Jokinen, H. Rahiala, M. Pääsi, J. Heikkilä, I. Kangasniemi and A. Yli-Urpo, *J. Biomed. Mater. Res.*, **51**, 200–208 (2000).
- 4) P. Li, C. Ohtsuki, T. Kokubo, K. Nakanishi, N. Soga, T. Kanamura and T. Yamamuro, *J. Am. Ceram. Soc.*, **75**, 2094–2097 (1992).
- 5) H.-M. Kim, T. Kokubo, S. Fujibayashi, S. Nishiguchi and T. Nakamura, *J. Biomed. Mater. Res.*, **52**, 553–557 (2000).
- 6) H.-M. Kim, H. Takadama, F. Miyaji, T. Kokubo, S. Nishiguchi and T. Nakamura, *J. Mater. Sci.: Mater. Med.*, **11**, 555–559 (2000).
- 7) T. Kokubo, H.-M. Kim and M. Kawashita, *Biomaterials*, **24**, 2161–2175 (2003).
- 8) P. Li, C. Ohtsuki, T. Kokubo, K. Nakanishi, N. Soga, T. Nakamura, T. Yamamuro and K. de Groot, *J. Biomed. Mater. Res.*, **28**, 7–15 (1994).
- 9) A. Oyane, M. Kawashita, T. Kokubo, M. Minoda, T. Miyamoto and T. Nakamura, *J. Ceram. Soc. Japan*, **110**, 248–254 (2002).
- 10) M. Uchida, H.-M. Kim, T. Kokubo, S. Fujibayashi and T. Nakamura, *J. Biomed. Mater. Res.*, **64A**, 164–170 (2003).
- 11) M. Keshmiri and T. Troczynski, *J. Non-Cryst. Solids*, **324**, 289–294 (2003).
- 12) S. Nishiguchi, T. Nakamura, H. Kato, H. Fujita, H. M. Kim, F. Miyaji and T. Kokubo, *J. Biomed. Mater. Res.*, **48**, 689–696 (1999).
- 13) S. Nishiguchi, H. Kato, M. Neo, M. Oka, H.-M. Kim, T. Kokubo and T. Nakamura, *J. Biomed. Mater. Res.*, **54**, 198–208 (2001).
- 14) J. Lee, Y. J. Oh, S. K. Lee and K. Y. Lee, *J. Controlled Release*, **146**, 61–67 (2010).
- 15) T. Kokubo, H. Kushitani, S. Sakka, T. Kitsugi and T. Yamamuro, *J. Biomed. Mater. Res.*, **24**, 721–734 (1990).
- 16) T. Kokubo and H. Takadama, *Biomaterials*, **27**, 2907–2915 (2006).
- 17) Z. Li, M. Kawashita, N. Araki, M. Mitsumori, M. Hiraoka and M. Doi, *Biomed. Mater.*, **5**, 065010 (2010) doi:10.1088/1748-6041/5/6/065010.
- 18) K. M. S. Khalil and S. A. Makhlof, *Appl. Surf. Sci.*, **254**, 3767–3773 (2008).
- 19) T. Kokubo, T. Ueda, M. Kawashita, Y. Ikuhara, G. H. Takaoka and T. Nakamura, *J. Mater. Sci.: Mater. Med.*, **19**, 695–702 (2008).
- 20) X. X. Wang, S. Hayakawa, K. Tsuru and A. Osaka, *Biomaterials*, **23**, 1353–1357 (2002).
- 21) Y. Suyama and A. Kato, *Yogyo-Kyokai-Shi*, **86**, 120–125 (1978).
- 22) X. Liu and C. Ding, *Mater. Lett.*, **57**, 652–655 (2002).
- 23) Y. Leng, J. Chen and S. Qu, *Biomaterials*, **24**, 2125–2131 (2003).
- 24) R. Z. LeGeros and J. P. LeGeros, in: L. L. Hench, J. Wilson (Eds.), “An Introduction to Bioceramics”, World Scientific, Singapore (1993) p. 145.
- 25) H.-M. Kim, T. Himeno, M. Kawashita, T. Kokubo and T. Nakamura, *J. R. Soc., Interface*, **1**, 17–22 (2004).
- 26) W. Wu and G. H. Nancollas, *J. Colloid Interface Sci.*, **199**, 206–211 (1998).
- 27) P. Li, I. Kangasniemi, K. de Groot and T. Kokubo, *J. Am. Ceram. Soc.*, **77**, 1307–1312 (1994).
- 28) H. Takadama, H.-M. Kim, T. Kokubo and T. Nakamura, *J. Biomed. Mater. Res.*, **57**, 441–448 (2001).
- 29) C. Zener, *J. Appl. Phys.*, **20**, 950–953 (1949).
- 30) F. Liang, L. Zhou and K. Wang, *Surf. Coat. Tech.*, **165**, 133–139 (2003).